Materials Science Forum
ISSN: 1662-9752, Vol. 1190, pp 69-77
doi:10.4028/p-9ppZEB

Submitted: 2025-09-28
Revised: 2026-01-07
Accepted: 2026-01-31
Online: 2026-05-18

Synchrotron X-Ray Topography Analysis of Low Angle Grain Boundaries Induced by Growth Step Flow in PVT-Grown 4H-SiC Crystals

Jianpei Zhang[1,a], Zeyu Chen[1,b], Yuzhuo LI[1,c], Shanshan Hu[1,d], Balaji Raghothamachar[1,e], Yafei Liu[2,f], Campbell Bouch[2,g], Ryan Philpott[2,h], Scott Turchetti[2,i], Pete Schunemann[2,j] and Michael Dudley[1,k,*]

[1]Department of Materials Science & Chemical Engineering, Stony Brook University, Stony Brook, NY 11794 USA

[2]Onsemi, 55 Executive Drive, Hudson, NH 03051 USA

[a]Jianpei.zhang@stonybrook.edu, [b]Zeyu.cheni@stonybrook.edu, [c]Yuzhou.Li@stonybrook.edu, [d]Shanshan.hu@stonybrook.edu, [e]Balaji.ragnothamachar@stonybrook.edu, [f]Yafei.Liu@onsemi.com, [g]Campbell.Bouch@onsemi.com, [h]Ryan.Philpott@onsemi.com, [i]Scott.Turchetti@onsemi.com, [j]Pete.Schunemann@onsemi.com, [k]Michael.Dudley@stonybrook.edu,

Keywords: 4H-Silicon carbide, physical vapor growth, low-angle grain boundary, synchrotron x-ray characterization.

Abstract. Synchrotron X-ray topography (XRT) combined with ray-tracing simulation was employed to examine the distribution and formation mechanisms of LAGBs in off-axis 4H-SiC wafers grown by PVT. TED-LAGB networks were observed adjacent to the facet, along with three TED-LAGBs emanating from micropipes on the left edge of the wafer. Ray-tracing simulations enabled the identification of TED Burgers vectors by correlating simulated and observed contrast configurations. The results suggest that large TED-LAGB networks near facets originate from misorientations between growth fronts of horseshoe-shaped steps incorporating prismatic slip dislocations, induced by radial temperature gradients. Similarly, LAGBs associated with micropipes arise from localized step-flow perturbations. These findings provide a revised mechanism for TED-LAGBs formation, establishing a link between their spatial distribution and growth dynamics, and offering new insights into their role in determining the quality of 4H-SiC substrates.

Introduction

Silicon carbide (SiC) is a wide-bandgap semiconductor with high breakdown field and strong electrical and thermal conductivity[1]. These properties make it an important material for modern power and electronic systems, such as inverters, on-board chargers, and converters for electric vehicles[2], [3]. However, the presence of defects in PVT-grown SiC crystals negatively affect the reliability and performance of SiC devices. Among various types of defects in SiC crystals, low-angle grain boundaries (LAGBs) are a commonly observed planar defect that limit yield and prevent the implementation of large SiC devices[4]. LAGBs form through the aggregation of different types of dislocations, usually threading edge dislocations (TEDs) or edge type basal plane dislocations (BPDs) to accommodate the misorientation of lattice planes[5]. TED-LAGBs lead to tilt along prismatic planes often associated with radial temperature gradients and the coalescence of growth steps, forming network-like structures across the wafer and producing noticeable lattice tilt. BPD-LAGBs, on the other hand, result from the aggregation of basal plane dislocations (BPDs), particularly those of opposite signs driven together under stress, giving rise to tilt of the basal plane[5]. These boundaries are usually found near wafer edges or stress-concentrated regions and can sometimes combine with TED arrays to form composite grain boundary structures. They are more likely to evolve into Shockley stacking faults during device operation, severely impacting the performance

and reliability of power devices[6, 7]. Classical formation mechanisms of <1$\bar{1}$00> orientation LAGBs are generally associated with threading screw dislocations (TSDs), which act as growth centers by generating spiral steps[8]. TED-LAGBs formed as TEDs align along the <1$\bar{1}$00> direction to accommodate the c-axis rotation between the TSDs and surrounding regions when growth centers converge. Step flow based mechanism was proposed by Cheng et al[9] indicating that radial temperature gradients drive horseshoe-shaped step flow from the facet, where merging fronts incorporate prismatic slip dislocations to form TED-LAGBs.

In this study, an unique distribution patterns of LAGBs observed in physical vapor transport (PVT) grown off-axis 4H-SiC wafers is investigated. Synchrotron X-ray topography (XRT) in both transmission and grazing geometry reveal the presence of LAGBs networks next to the facet regions as well as associated with micropipes on the left edge of the wafer. A systematic analysis has been carried out to identify the dynamics of step flow and the associated mechanisms of LAGB formation induced by its motion.

Experiment

4H-SiC wafers grown by physical vapor transport (PVT) method with a 4° offcut were characterized by synchrotron x-ray topography (XRT)[10]. Both transmission and grazing-incidence geometries were employed, with topographs recorded under white-beam and monochromatic conditions, respectively. Synchrotron white beam x-ray topography (SWBXT) was recorded in a 11$\bar{2}$0 reflection with the Si face as the beam exit surface. Synchrotron monochromatic beam x-ray topography (SMBXT) was recorded in 11$\bar{2}$8 from the Si face of the wafer. Experiments were conducted at the Advanced Photon Source (APS) in the Argonne National Laboratory (ANL). Ray-tracing simulation was carried out based on the orientation contrast mechanism[11] for Burgers vector analysis of observed dislocations.

Results and Discussion

TED-LAGB Network adjacent to the Facet. Schematic diagram shows the location of LAGB networks of the wafer indicated by the red lines (Fig. 1a). SMBXT recorded from the Si face of the wafer reveals this LAGB network consists of numerous black and white contrast TED-LAGB arrays each extending along the <1$\bar{1}$00> directions which are marked with red lines. The optical image of the PVT-grown off-axis 4H-SiC wafer shows an unusual shape of the facet outlined with red line with three spikes along the <11$\bar{2}$0> directions which are marked with green lines (Fig. 1c). In the facet regions, a star pattern that is also marked with green lines is observed with each line also following <11$\bar{2}$0> directions, indicating that the spikes correspond to this star pattern (Fig. 1d). The SMBXT image recorded from the Si face of the wafer reveals a micropipe at the center of the star pattern marked with a red arrow in fig. 1e which is also crossing point of three spike. Similar pattern was reported by M. Sonoda et al[13], where the facet region showed hexagonal symmetry comprising six vicinal (000$\bar{1}$) C surfaces tilted toward <1$\bar{1}$00> directions, indicating that these spikes originagte from the micropipe which act as the growth center during PVT growth.

To investigate the nature of dislocations comprising the LAGB network, ray-tracing-simulated TEDs with different Burgers vectors in the <11$\bar{2}$8> reflection are compared with actual topographic observations. Simulation reveals distinct contrast configuration variation of TEDs with six different a-component Burgers vectors shown in Fig. 2 [12]. They appear as either dark contrast TEDs (Fig. 2a and b) or white contrast. TEDs with a distorted white center decorated by two dark arcs (Fig. 2c-f). The Burgers vector of TEDs are perpendicular to the direction of each boundary.

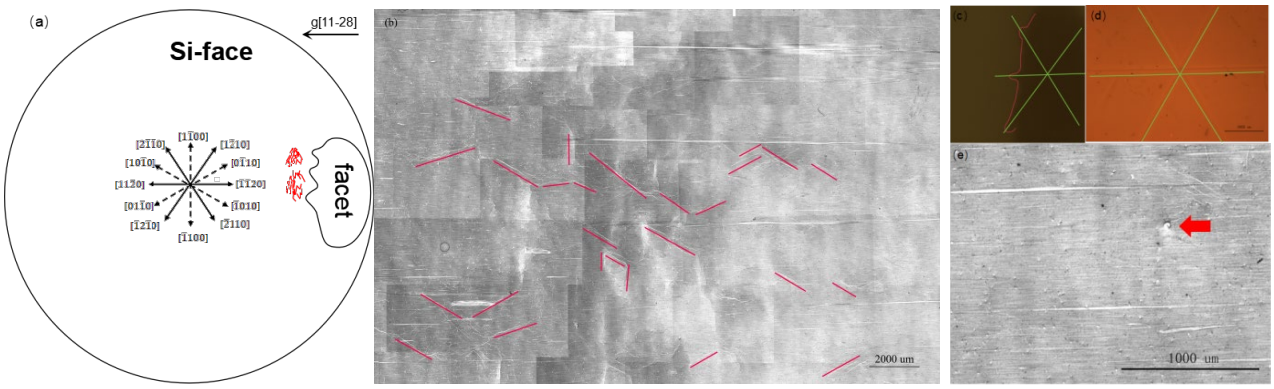

Fig. 1. (a) Schematic diagram shows the location of LAGB networks of the wafer indicated by red lines. (b) 11$\bar{2}$8 SMBXT image recorded from the Si face showing the presence of a large TED-LAGB network noted with red lines. (c) Optical image of the wafer shows unusual shape of facet outlined with red line and three spikes coming from the facet indicated by green lines. (d) Optical image of the star pattern marked with green lines corresponding to these spikes.(e) Micropipe at the center of the star pattern noted with red arrow.

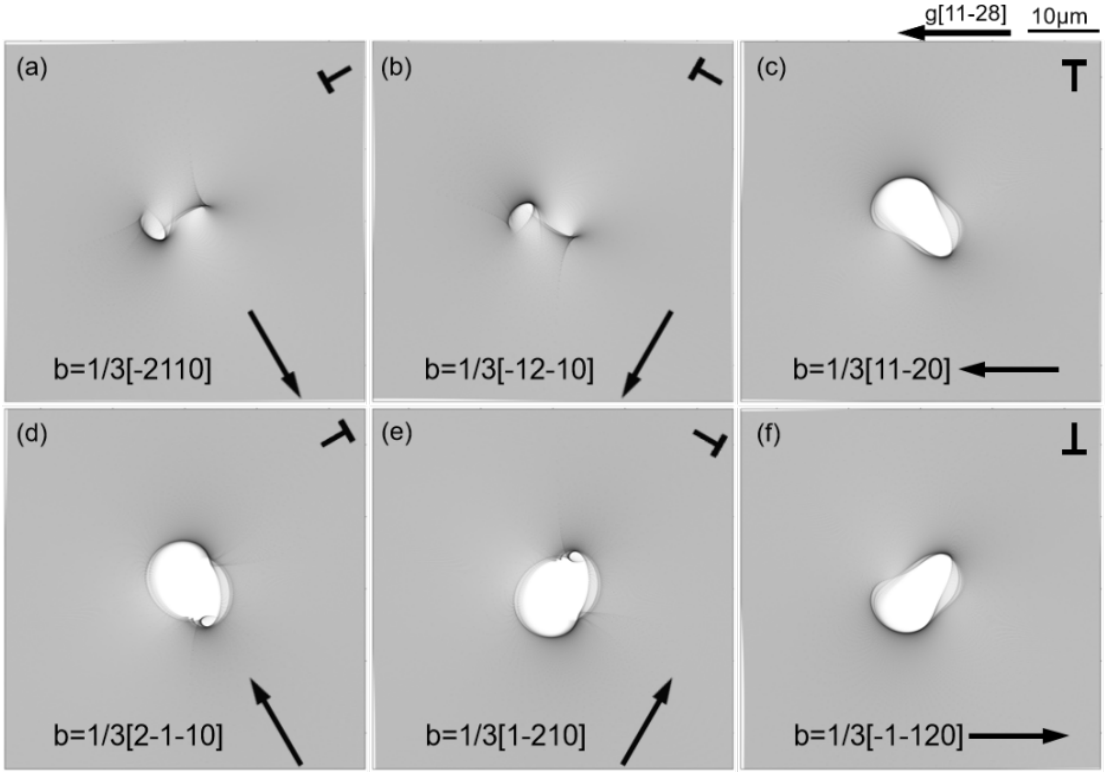

Fig. 2. Ray-tracing simulated 11$\bar{2}$8 grazing-incidence x-ray topographs of TEDs with six different a-component Burgers vectors [(a)–(f)] in 4H-SiC[12].

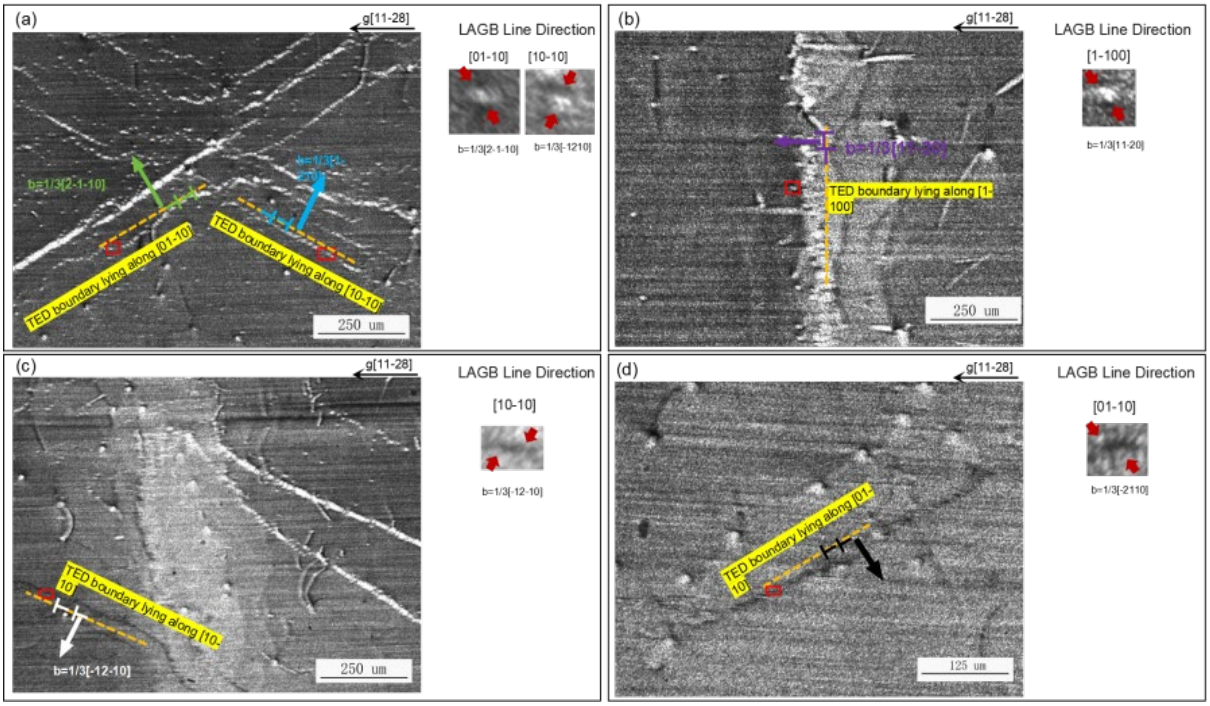

Fig. 3. Enlarged images of the TED-LAGB networks observed in 11$\bar{2}$8 SMBXT recorded from the Si face. Directions of TED arrays composing the LAGB network are highlighted by dotted lines. Contrasts of individual dislocations in each array marked with red boxes are enlarged showing that LAGBs along different <1$\bar{1}$00> are composed of TEDs with different contrast and Burgers vectors in (a), (b), (c) and (d).

Fig. 3 shows enlarged sections of these TED-LAGBs extending along all <1$\bar{1}$00> directions. For the white TED boundary lying along [01$\bar{1}$0], the enlarged image reveals that each TED with a white centered contrast has its top black contrast shifted more to the left and the bottom black contrast shifted more to the right. This configuration corresponds to the TED with Burgers vector b=1/3[2$\bar{1}\bar{1}$0] (Fig. 3a). For the white TED boundary lying along [10$\bar{1}$0], the enlarged image indicates that each white centered TED has its top black contrast shifted to the right and the bottom black contrast shifted to the left, which corresponds to a TED with Burgers vector b=1/3[1$\bar{2}$10] (Fig. 3a). For the white TED boundary lying along [1$\bar{1}$00], the enlarged image shows that each white centered TED has a larger top portion than bottom, top black contrast shifted to the left and the bottom black contrast shifted to the right, which corresponds to a TED with Burgers vector b=1/3[11$\bar{2}$0] (Fig. 3b). For the black TED boundary lying along [10$\bar{1}$0], the enlarged image shows that each black centered TED has its top black arc shifted to the left side and bottom black arc shifts to the right side, which corresponds to a TED with Burgers vector b= 1/3[$\bar{1}$2$\bar{1}$0] (Fig. 3c). For the black TED boundary lying along [01$\bar{1}$0], the enlarged image shows that each black centered TED has its top black arc shifted to the right side and bottom black arc shifted to the left side, which corresponds to a TED with Burgers vector b= 1/3[$\bar{2}$110] (Fig. 3d).

Formation mechanism of TED LAGB Network adjacent to the Facet. A horseshoe-shaped growth step model to explain the TED LAGB network formation on PVT-grown 4H-SiC wafer was proposed by Cheng et al[9]: The crucible design of PVT growth has the heating induction coils encircling the growth cell, creating a radial temperature difference between the inner and outer region of the crystal, which temperature on the edge is higher than it on the center region. This causes diffusivity differences in adatoms deposited at various locations on the growth interface. Faster growth rate is expected at higher growth temperature[16]. Besides, higher growth temperatures

promote a smooth step morphology with smaller step heights, while lower temperatures increase step height and form large terraces, which introduce propagation speed variation during growth[17]. Observation of step morphology on initial grown 4H-SiC crystals reveals that steps originate from the growth facet position and propagate across the crystal radially[18]. Above all, step front near the crystal edge propagates faster than in the central region, a horseshoe-shaped growth step is formed.

The primary TED source of TED-LAGB networks is pre-existing prismatic slip dislocations in the adjacent regions [19]. Such dislocations are typically deformation-induced and arise from activation of the secondary slip system 1/3 <11$\bar{2}$0> {1$\bar{1}$00}. The key factor enabling the activation of prismatic slip in 4H-SiC during PVT growth is thermal stress generated by the radial temperature gradients, which applies shear stress to all slip systems according to Schmid's law. Gliding of pre-existing TEDs on the secondary prismatic slip system will occur once the resolved shear stress exceeds the critical resolved shear stress (CRSS). This interpretation of having prismatic slip dislocations as the LAGB network dislocation source can be further verified by analyzing the prismatic slip dislocation distribution prediction model developed by Guo et al.[14]. in conjunction with ray-tracing simulation. Guo et al.'s study revealed screw-oriented prismatic slip dislocation segments as distinct straight linear contrast along one of the three [11$\bar{2}$0] directions in synchrotron x-ray topographs near the periphery of 4H-SiC wafers[14]. Therefore, the horseshoe-shaped growth step incorporates prismatic slip dislocations to form LAGBs at its encountering location as the mobile TED segment glides behind the growth front and leaves a screw-oriented prismatic slip dislocation segment in its wake. Before the faces of the two growth fronts encounter each other, the original TED segment will escape the coalescing front, leaving a surface intersecting point of the screw-oriented prismatic slip dislocation segment. When the steps merge, in order to enable conservation of Burgers vector, the prismatic dislocations will be forced to redirect into TEDs exiting the top surface.

An analogous interpretation can be made for the LAGB network adjacent to the facet. Three spikes of facet emerging from the MP in the facet (Fig. 1(e)) extend along the [11$\bar{2}$0] directions (Fig. 4a). Due to the radial temperature gradient between the center and edge of the wafer, atoms deposited onto the terrace of the growth steps exhibit different diffusivities. Spikes closer to the edges of the boule propagate faster than the one between them, forming horseshoe shaped growth fronts on both sides. As growth continues, opposing spike fronts from each side converge first near the facet region, roughly along the horizontal direction (Fig. 4b-c). TED on the growth fronts will glide along [1$\bar{2}$10] and [$\bar{1}$2$\bar{1}$0] directions on the prismatic plane to form TED-LAGBs along [01$\bar{1}$0] and [10$\bar{1}$0] directions. The central spike will keep moving forward and it will encounter with other fronts on sides initially. As the central spike continues to advance, it will encounter the side fronts. To accommodate the misorientation introduced by the side front induced TED-LAGBs, the TED-LAGBs along the [1$\bar{1}$00] direction will be formed(Fig. 4d). Each growth front undergoes this process, but due to changes in growth conditions process, the step flow pattern may slightly differ resulting in the formation of TED-LAGB networks in this region (Fig. 4e).

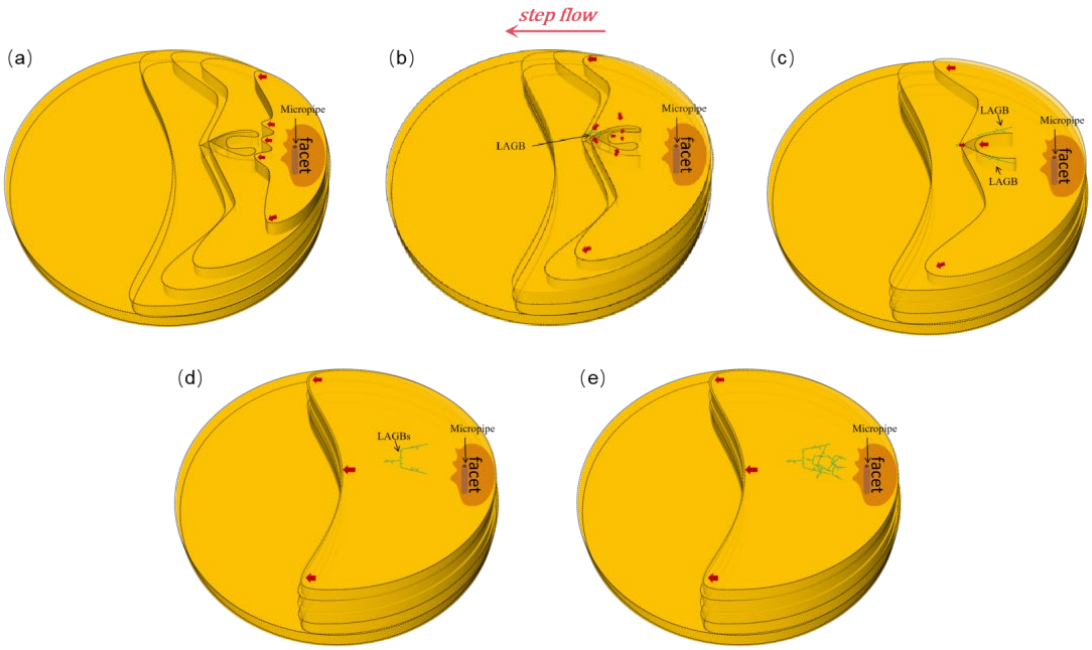

Fig. 4. Schematic diagrams showing the formation mechanism of TED-LAGB networks coming from spikes based on the horse-shoe shape step flow mechanism.

TED-LAGB from Micropipes. Beyond the facet region, synchrotron XRT reveals LAGBs emanating from micropipes on the PVT-grown off-axis 4H-SiC wafer. Schematic diagram shows the location of LAGBs indicated by the blue lines(Fig. 5d). The SMBXT images (Fig.5a-c) reveals that these LAGBs noted with blue lines consisting very high density black or white contrast TED-LAGB arrays originates from contrasts associated with micropipes or micropipe arrays marked with green boxes. Optical images of MPs and MP arrays corresponding to those contrasts are observed indicated by green lines.

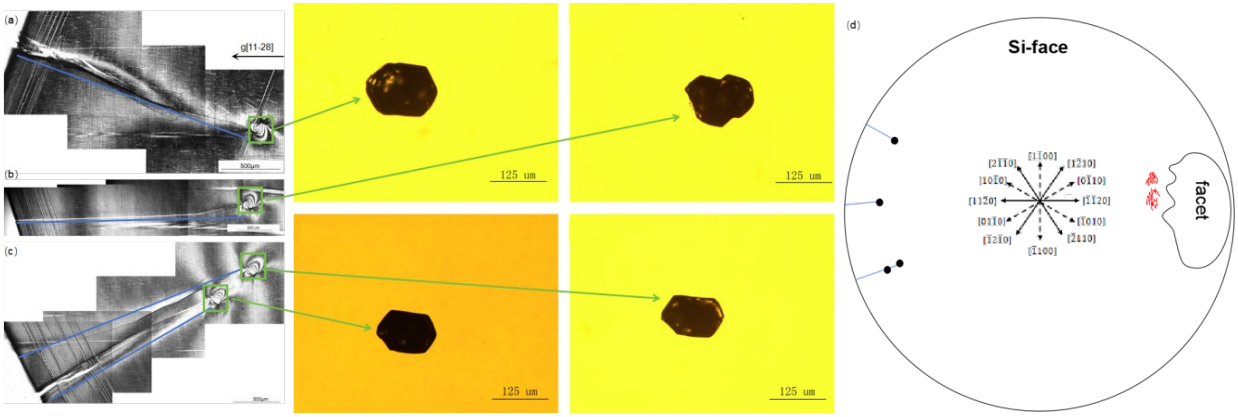

Fig. 5. $11\bar{2}8$ Grazing-incidence synchrotron monochromatic beam x-ray topograph recorded from the Si face showing the presence of TED-LAGBs originating from micropipes marked with blue lines(a-c). The location of TED-LAGBs of the wafer indicated by the blue lines are shown on (d).

Formation mechanism of TED-LAGB from Micropipes. Based on these observations and horseshoe-shaped growth step model, we proposed a formation mechanism for LAGBs originating from MPs in the PVT-grown off-axis 4H-SiC boule in this study. Step flows merge together after the formation of TED-LAGBs near the facet and continue to propagate radially outward to other side of boule. When a MP is encountered, the step flow is pinned by the MP and the direction of the step flow changes to form a horseshoe-shaped growth step around the MP. When the two horse-shoe shaped growth fronts merge together, the pre-existing TEDs in this region will glide on the secondary

prismatic slip system to accommodate the misorientation between the fronts when the resolved shear stress exceeds the CRSS.When more growth steps accumulate during growth, each one undergoes this process repeatedly, but due to changes in growth conditions process, the step flow pattern may slightly differ from layer to layer resulting in the LAGB network adjacent to the MP cluster.

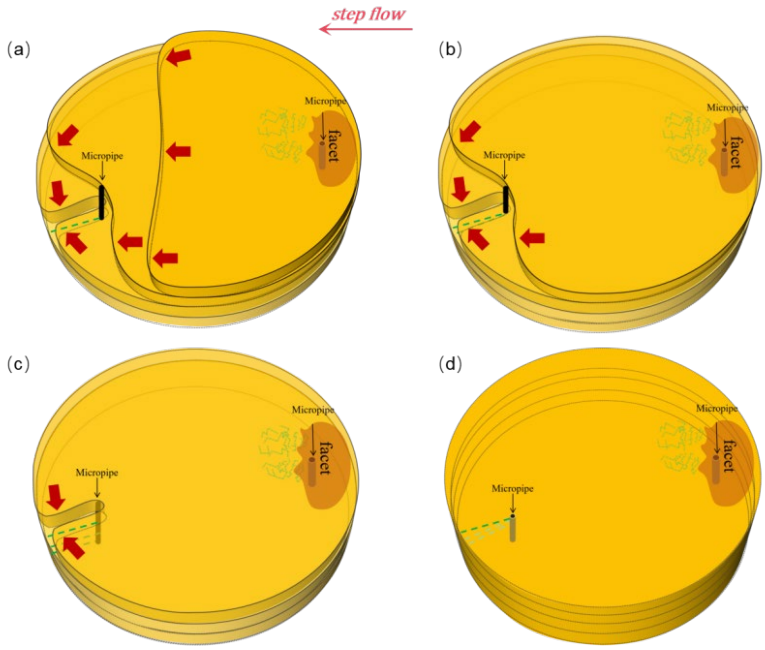

Fig. 6. Schematic diagrams showing the formation mechanism of TED-LAGBs coming from micropipes based on the horse-shoe shape step flow mechanism.

Summary

In this work, synchrotron X-ray topography and ray-tracing simulation are employed to investigate the distribution and formation mechanisms of LAGBs in PVT-grown 4H-SiC crystal. TED-LAGB networks next to the facet and three TED-LAGBs emanating from MPs are observed. Ray-tracing simulations enabled the identification of Burgers vectors of TEDs in these LAGBs from contrast configurations observed in synchrotron topographs. The results indicate that TED-LAGB networks next to the facet form to accommodate the misorientation between growth fronts of horseshoe-shaped steps, which incorporate prismatic slip dislocations originating from facet spikes under radial temperature gradients during growth. For TED-LAGBs emanating from micropipes, the MPs act as localized centers that also redirect step flows into horseshoe-shaped steps, thereby generating TED-LAGBs to accommodate the misorientation of those steps. Based on these observations, the role of step-flow dynamics and dislocation interactions in LAGB development is highlighted. These findings provide new insight into the origin of LAGBs in SiC crystals and their implications for substrate quality.

Acknowledgement

Work was supported by Onsemi. Research used resources of the Advanced Photon Source (Beamline 1-BM), a U.S. DOE Office of Science User Facility operated for the DOE Office of Science by Argonne National Laboratory under Contract No. DE-AC02-06CH11357. This research used resources of the National Synchrotron Light Source II, a U.S. Department of Energy (DOE) Office of Science User Facility operated for the DOE Office of Science by Brookhaven National Laboratory under Contract No. DE-SC0012704. The Joint Photon Sciences Institute at SBU provided partial support for travel and subsistence at the Advanced Photon Source.

References

[1] L. F. S. Alves *et al.*, "SIC power devices in power electronics: An overview," in *2017 Brazilian Power Electronics Conference (COBEP)*, Juiz de Fora: IEEE, Nov. 2017, pp. 1–8. doi: 10.1109/COBEP.2017.8257396.

[2] M. Dudley, S. Wang, W. Huang, C. H. Carter, V. F. Tsvetkov, and C. Fazi, "White-beam synchrotron topographic studies of defects in 6H-SiC single crystals," *J. Phys. Appl. Phys.*, vol. 28, no. 4A, pp. A63–A68, Apr. 1995, doi: 10.1088/0022-3727/28/4a/012.

[3] X. R. Huang, M. Dudley, W. M. Vetter, W. Huang, W. Si, and C. H. Carter Jr, "Superscrew dislocation contrast on synchrotron white-beam topographs: an accurate description of the direct dislocation image," *J. Appl. Crystallogr.*, vol. 32, no. 3, pp. 516–524, Jun. 1999, doi: 10.1107/S0021889899002939.

[4] Y. Chen, H. Chen, N. Zhang, M. Dudley, and R. Ma, "Investigation of Low Angle Grain Boundaries in Hexagonal Silicon Carbide," *MRS Proc.*, vol. 955, pp. 0955-I07-50, 2006, doi: 10.1557/PROC-0955-I07-50.

[5] Y. Chen, G. Dhanaraj, W. M. Vetter, R. H. Ma, and M. Dudley, "Behavior of Basal Plane Dislocations and Low Angle Grain Boundary Formation in Hexagonal Silicon Carbide," *Mater. Sci. Forum*, vol. 556–557, pp. 231–234, Sep. 2007, doi: 10.4028/www.scientific.net/MSF.556-557.231.

[6] M. Dudley *et al.*, "Formation Mechanism of Stacking Faults in PVT 4H-SiC Created by Deflection of Threading Dislocations with Burgers Vector c+a," *Mater. Sci. Forum*, vol. 679–680, pp. 269–272, Mar. 2011, doi: 10.4028/www.scientific.net/MSF.679-680.269.

[7] M. Dudley *et al.*, "Stacking faults created by the combined deflection of threading dislocations of Burgers vector c and c+a during the physical vapor transport growth of 4H–SiC," *Appl. Phys. Lett.*, vol. 98, no. 23, p. 232110, Jun. 2011, doi: 10.1063/1.3597226.

[8] F. Z. Wu *et al.*, "Synchrotron X-Ray Topography Studies of the Propagation and Post-Growth Mutual Interaction of Threading Growth Dislocations with C-Component of Burgers Vector in PVT-Grown 4H-SiC," *Mater. Sci. Forum*, vol. 717–720, pp. 343–346, May 2012, doi: 10.4028/www.scientific.net/MSF.717-720.343.

[9] Q. Cheng, Z. Chen, S. Hu, B. Raghothamachar, and M. Dudley, "Analysis of Threading Edge Dislocation Low-Angle Grain Boundary Network Distributions in 4H-SiC Wafers Through Synchrotron X-ray Topography and Ray-Tracing Simulation," *J. Electron. Mater.*, Feb. 2025, doi: 10.1007/s11664-025-11793-y.

[10] T. Ailihumaer *et al.*, "Synchrotron X-ray Topography Studies of Dislocation Behavior During Early Stages of PVT Growth of 4H-SiC Crystals," *J. Electron. Mater.*, vol. 50, no. 6, pp. 3258–3265, Jun. 2021, doi: 10.1007/s11664-021-08827-6.

[11] T. Ailihumaer *et al.*, "Surface relaxation and photoelectric absorption effects on synchrotron X-ray topographic images of dislocations lying on the basal plane in off-axis 4H-SiC crystals," *Mater. Sci. Eng. B*, vol. 271, p. 115281, Sep. 2021, doi: 10.1016/j.mseb.2021.115281.

[12] Q. Cheng, Z. Chen, S. Hu, Y. Liu, B. Raghothamachar, and M. Dudley, "Analysis of dislocation configurations in SiC crystals through X-ray topography aided by ray tracing simulations," *Mater. Sci. Semicond. Process.*, vol. 174, p. 108207, May 2024, doi: 10.1016/j.mssp.2024.108207.

[13] M. Sonoda, T. Nakano, K. Shioura, N. Shinagawa, and N. Ohtani, "Structural characterization of the growth front of physical vapor transport grown 4H-SiC crystals using X-ray topography," *J. Cryst. Growth*, vol. 499, pp. 24–29, Oct. 2018, doi: 10.1016/j.jcrysgro.2018.07.029.

[14] J. Guo *et al.*, "Prismatic Slip in PVT-Grown 4H-SiC Crystals," *J. Electron. Mater.*, vol. 46, no. 4, pp. 2040–2044, Apr. 2017, doi: 10.1007/s11664-016-5118-9.

[15] S. Hu *et al.*, "Characterization of Prismatic Slip in SiC Crystals by Chemical Etching Method," *Mater. Sci. Forum*, vol. 1089, pp. 45–50, May 2023, doi: 10.4028/p-6dx2v3.

[16] T. Okamoto *et al.*, "Quality Evaluation of 150 mm 4H-SiC Grown at over 1.5 mm/h by High-Temperature Chemical Vapor Deposition Method," *Solid State Phenom.*, vol. 342, pp. 105–112, May 2023, doi: 10.4028/p-09h52t.

[17] T. Kimoto and H. Matsunami, "Surface diffusion lengths of adatoms on 6H-SiC{0001} faces in chemical vapor deposition of SiC," *J. Appl. Phys.*, vol. 78, no. 5, pp. 3132–3137, Sep. 1995, doi: 10.1063/1.359999.

[18] N. Ohtani *et al.*, "Investigation of heavily nitrogen-doped n+ 4H–SiC crystals grown by physical vapor transport," *J. Cryst. Growth*, vol. 311, no. 6, pp. 1475–1481, Mar. 2009, doi: 10.1016/j.jcrysgro.2009.01.119.

[19] S. Hu *et al.*, "Characterization of prismatic slip in PVT-grown AlN crystals," *J. Cryst. Growth*, vol. 584, p. 126548, Apr. 2022, doi: 10.1016/j.jcrysgro.2022.126548.